sideration of wave propagation can also produce one other relationship, $P=\Delta s/U$, where U is the freestream velocity.

In practice one should use the *maximum* value of the two periods. In most engineering problems $\Delta s/U$ will be maximum. This restriction limits the resolution of numerical frequencies to those below a value of $f_{max}=1/P_{max}$.

In summary, the use of the Reynolds-averaged equations for numerically solving time-dependent flows implies an averaging over an interval P that is related to the step size of the numerical grid.

Empirical Reynolds Stress

With this strategy, requirements can be imposed upon the experimental determination of Reynolds' stresses. Measured values of $u'v'$ are required to model turbulence. This can be accomplished (admittedly with great difficulty) by use of a hot-wire anemometer or laser Doppler velocimeter. When two wire hot-film anemometers are used, Reynolds stress components can be obtained by using the ac voltage output, which corresponds to mass flux per unit area, from the two wires. For example,

$$\overline{u'v'}=k(\overline{e_1^2}-\overline{e_2^2}) \tag{9}$$

where e_1 and e_2 are the ac voltage outputs from the two wires and the constant $k=0.5/\rho^2$. From these data a spectral analysis of $u'v'$ can be performed and the Fourier components ascertained for a wide range of frequencies. By recording $u'v'$ vs time and employing a harmonic analyzer the important Fourier components may be extracted.

A typical power spectral density plot of these coefficients is shown in Fig. 1 where the usual definition is

$$\overline{u'v'}=\int_0^\infty \frac{\mathrm{d}(\overline{u'v'})}{\mathrm{d}f}\,\mathrm{d}f \tag{10}$$

For the numerical analysis only the Reynolds' stresses for the frequency range above $f=1/P_{max}$ are of interest, since those frequencies below $1/P_{max}$ are captured by the numerical solution. Hence $\overline{u'v'}$ is redefined for numerical calculation as

$$\overline{\overline{u'v'}}=\int_{1/P}^\infty \frac{\mathrm{d}(\overline{u'v'})}{\mathrm{d}f}\,\mathrm{d}f \tag{11}$$

This integral represents only the higher end of the frequency spectrum shown in Fig. 1. The lower end of the spectrum will be computed using the complete Navier-Stokes equations.

A very important parameter used for unsteady turbulent flows is the Strouhal number defined as $St_A=fA/U$ where f is the frequency of the disturbance, U the freestream or uniform flow velocity, and A a dimension that, for bodies of revolution, is usually the body diameter D or, for unsteady flows, can be the shear layer thickness δ. The power spectral density for the Reynolds stresses can be plotted vs the Strouhal number, as shown in Fig. 2.

From previous experimental results, it is known that most of the turbulent energy is concentrated in the Strouhal number range $St_D=0$-0.6 for most configurations. In the wake of a two-dimensional circular cylinder, the maximum Strouhal number St_D recorded is 0.21. For ogive cylinders at high angles of attack most of the energy in the wake is concentrated at $0.2\le St_D\le 0.6$ for freestream Mach numbers up to 3 and cross-flow Mach numbers up to 2.[1] Self-excited shock oscillations on spike-tipped bodies of revolution placed at zero angle of attack in a supersonic flow at Mach 3 generate a Strouhal number St_D of about 0.2 (Ref. 2) and of about 0.22 for the experimental configuration of Ref. 3. Self-excited wave oscillations generated in water on similar two-dimensional spike-tipped bodies have a Strouhal number based on spike length $St_L=0.16$, while oscillations generated in air and water over rectangular cavities have $St_L=0.3$.[4]

If a Strouhal number based on shear-layer thickness St_δ were used as a parameter, most of the turbulent energy would be concentrated in a Strouhal number range one order of magnitude smaller than for St_D. For example, for the spike-tipped body experiment of Ref. 3, St_D is equal to 0.22 while St_δ is equal to 0.02 for maximum oscillations. The shock oscillations subside for $St_\delta=0.04$. Thus, most turbulent flows must have a stress distribution where the energy is concentrated at $St_\delta<1.0$. Then, if $St_\delta\ll 1.0$, this condition is analogous to a state of "frozen" turbulence and the total value of the eddy viscosity should be used in the Reynolds-averaged equations. Conversely, a condition where $St_\delta\gg 1$ is analogous to "equilibrium" turbulence and the eddy viscosity value used should be zero.

Conclusion

To analyze unsteady turbulent flows, the Reynolds-averaged equations are used, *but* averaged over a period P which is related to the grid size,

$$P=\max \text{ of } \Delta t,\ \Delta s/U$$

Therefore the Reynolds' stress obtained from experiment and used in the numerical calculation is only that portion of the $u'v'$ frequency spectrum above the frequency $=1/P$,

$$\overline{\overline{u'v'}}=\int_{1/P}^\infty \frac{\mathrm{d}\overline{u'v'}}{\mathrm{d}f}\,\mathrm{d}f$$

Depending on the value of the Strouhal number based on the shear-layer thickness, the total experimental value of the eddy viscosity can be used in the equations if $St_\delta\ll 1$ and the eddy viscosity can be set equal to zero if $St_\delta\gg 1$. If $St_\delta=0(1)$, the correct frequency spectrum of the experimental value of the eddy viscosity must be used.

References

[1] Thomson, K. D. and Morrison, D. F., "The Spacing, Position and Strength of Vortices in the Wake of Slender Cylindrical Bodies at Large Incidence," *Journal of Fluid Mechanics*, Vol. 50, Pt. 4, 1971, pp. 751-783.

[2] Demetriades, A. and Hopkins, A. T., "Asymmetric Shock Wave Oscillations on Spike Bodies of Revolution," *Journal of Spacecraft and Rockets*, Vol. 13, Nov. 1976, pp. 703-704.

[3] Calarese, W., Hankey, W. L., and Shang, J. S., "Investigation of Self-Sustained Shock Oscillations on a Spike-Tipped Body at Mach 3," *Conference Proceedings on Computers in Flow Prediction and Fluid Dynamics Experiments*, Nov. 1981, ASME, New York, pp. 151-156.

[4] Calarese, W. and Hankey, W. L., "Self-Excited Wave Oscillations in a Water Table," *AIAA Journal*, Vol. 21, March 1983, pp. 372-378.

Buckling of Sinusoidally Corrugated Plates under Axial Compression

Susumu Toda*
National Aerospace Laboratory, Tokyo, Japan

Introduction

WIDELY used as a lightweight structure in a number of applications, the corrugated plate has usually been

Received Sept. 2, 1982.

*Senior Researcher. Member AIAA.

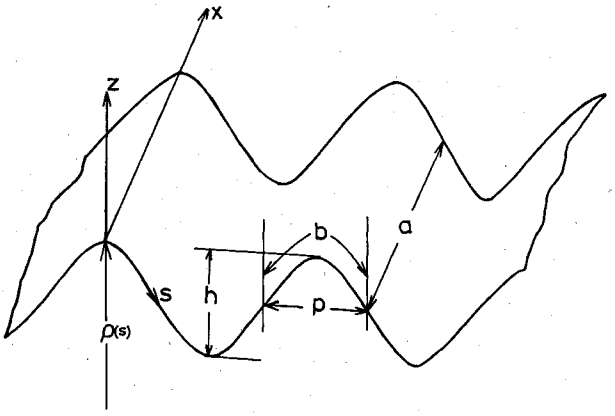

Fig. 1 Geometries and coordinate system.

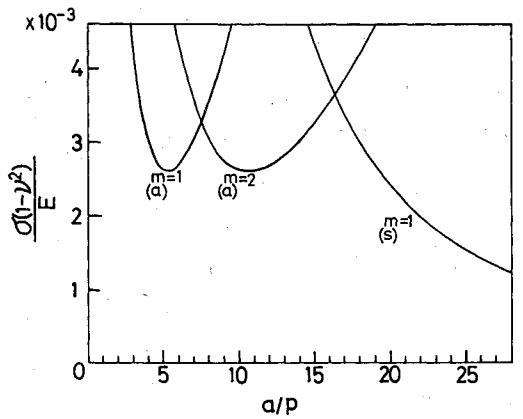

Fig. 2 Buckling characteristics of corrugated plates.

considered as an equivalent flat plate having orthotropic material properties[1] in theoretical buckling analysis. For the extreme case, however, when the number of corrugations is quite small or the plate length is very short, it is easy to anticipate that the orthotropic plate theory is not applicable. Hence, refined numerical studies of the buckling of corrugated plates recently have been undertaken by several researchers. For example, Libove and his students[1,2] have been investigating the shear buckling of both sinusoidally and trapezoidally corrugated plates, their analysis being based on the principle of minimum potential energy. Sanbongi has conducted a parametric numerical study using the high-precision finite strip element and has presented the results on the buckling of circularly corrugated plates under both axial compression[3] and shear.[4] However, additional analytical and experimental investigations seem to be required for a better understanding of the buckling behavior of corrugated plates.

The purpose of this Note is to present an analytical explanation of the buckling characteristics of sinusoidally corrugated plates under axial compression. Assuming that the buckling deflection components are in the form of a Fourier series, the second increment of the potential energy is evaluated with the aid of linear shell theory. Then the eigenvalue equations for neutral equilibrium are obtained by variations in the potential energy. Finally, an approximate but closed-form solution is presented for the critical axial compressive stress.

Theoretical Analysis

Consider a thin sinusoidally corrugated plate of isotropic material with Young's modulus E and Poisson's ratio ν. The coordinate system (x,s) is defined in the middle surface, such that x measures the axial distance along the generator and s is the arc length along the corrugation. The third coordinate z is taken in the normal direction. During the buckling of the plate under axial compressive stress σ, the deflection components in these directions are denoted u, v, and w, respectively. The geometry and the coordinate system of the analytical model for a corrugated plate with thickness t is shown in Fig. 1, where the radius of curvature $\rho(s)$ is defined by

$$1/\rho = (1/R)\cos(\pi s/b) \tag{1}$$

where R is the radius of curvature at the crests. The following geometric relations are easily derived

$$\frac{\pi p}{b} = \int_0^{\pi} \frac{1}{\sqrt{1+\kappa^2\sin^2\xi}}\,d\xi \equiv f_1$$
$$\frac{\pi h}{\kappa b} = \int_0^{\pi} \frac{\sin\xi}{\sqrt{1+\kappa^2\sin^2\xi}}\,d\xi \equiv f_2 \tag{2}$$

with

$$\kappa = b/\pi R \tag{3}$$

The second increment in the potential energy by transition from the unbuckled fundamental state to the buckled configuration at the same load is written in the form

$$P_2 = U_m + U_b + U_w \tag{4}$$

Here

$$U_m = \frac{Et}{2(1-\nu^2)}\int_0^a\int_0^{2b}\left[\left(\frac{\partial u}{\partial x}\right)^2 + \left(\frac{\partial v}{\partial s}+\frac{w}{\rho}\right)^2 + 2\nu\left(\frac{\partial u}{\partial x}\right)\left(\frac{\partial v}{\partial s}+\frac{w}{\rho}\right) + \frac{1-\nu}{2}\left(\frac{\partial u}{\partial s}+\frac{\partial v}{\partial x}\right)^2\right]dx\,ds \tag{5a}$$

$$U_b = \frac{Et^3}{24(1-\nu^2)}\int_0^a\int_0^{2b}\left[\left(\frac{\partial^2 w}{\partial x^2}\right)^2 + \left(\frac{\partial^2 w}{\partial s^2}\right)^2 + 2\nu\left(\frac{\partial^2 w}{\partial x^2}\right)\left(\frac{\partial^2 w}{\partial s^2}\right) + 2(1-\nu)\left(\frac{\partial^2 w}{\partial x\partial s}\right)^2\right]dx\,ds \tag{5b}$$

$$U_w = -\frac{\sigma t}{2}\int_0^a\int_0^{2b}\left[\left(\frac{\partial u}{\partial x}\right)^2 + \left(\frac{\partial v}{\partial x}\right)^2 + \left(\frac{\partial w}{\partial x}\right)^2\right]dx\,ds \tag{5c}$$

Let us assume a displacement field during buckling as

$$u = \cos\frac{m\pi x}{a}\sum_{n=0}^{\infty}\left(b_n\cos\frac{n\pi s}{b} + \bar{b}_n\sin\frac{n\pi s}{b}\right) \tag{6a}$$

$$v = \sin\frac{m\pi x}{a}\sum_{n=0}^{\infty}\left(c_n\sin\frac{n\pi s}{b} + \bar{c}_n\cos\frac{n\pi s}{b}\right) \tag{6b}$$

$$w = \sin\frac{m\pi x}{a}\sum_{n=0}^{\infty}\left(a_n\cos\frac{n\pi s}{b} + \bar{a}_n\sin\frac{n\pi s}{b}\right) \tag{6c}$$

which identically satisfy the boundary conditions specified by

$$w = \frac{\partial^2 w}{\partial x^2} = N_x = v = 0 \quad \text{at} \quad x=0 \text{ and } x=a \tag{7}$$

where N_x denotes the axial stress resultant.

Evaluating the integrals in Eqs. (5) and taking variation of P_2 with respect to a_n, $\bar{a}_n$, b_n, $\bar{b}_n$, c_n, and $\bar{c}_n$, we obtain two sets of governing equations, one for the symmetric and the other for the antisymmetric buckling mode with respect to the plane $s=0$.

Symmetric Buckling

Variation of P_2 with respect to a_n, b_n, and c_n yields an infinite number of linear homogeneous equations as follows:

$$F_{n-2}a_{n-2}/2+[A_n+\alpha(\phi_m^2+\psi_n^2)^2-\lambda_m]a_n+F_na_{n+2}/2 -\nu F_{n-1}\phi_m b_{n-1}-\nu F_n\phi_m b_{n+1}+F_{n-1}\psi_{n-1}c_{n-1} +F_n\psi_{n+1}c_{n+1}=0 \quad (n=0,1,2,\ldots) \quad (8)$$

$$-\nu F_{n-1}\phi_m a_{n-1}-\nu F_n\phi_m a_{n+1}+[\phi_m^2+(1-\nu)\psi_n^2/2-\lambda_m]b_n -(1+\nu)\phi_m\psi_n c_n/2=0 \quad (n=0,1,2,\ldots) \quad (9)$$

$$F_{n-1}\psi_n a_{n-1}+\psi_n a_{n+1}/2-(1+\nu)\phi_m\psi_n b_n/2 +[(1-\nu)\phi_m^2/2+\psi_n^2-\lambda_m]c_n=0 \quad (n=1,2,3,\ldots) \quad (10)$$

where

$$\phi_m=m\pi R/a, \quad \psi_n=n\pi R/b, \quad \alpha=t^2/12R^2$$

$$F_0=1, \quad F_n=\tfrac{1}{2} \quad (n=1,2,3,\ldots) \quad (11)$$

$$A_0=1, \quad A_1=\tfrac{3}{4}, \quad A_n=\tfrac{1}{2} \quad (n=2,3,4,\ldots)$$

and

$$\lambda_m=\lambda\phi_m^2 \text{ with } \lambda=\sigma(1-\nu^2)/E$$

The buckling load is determined by the smallest value of λ for which the homogeneous Eqs. (8-10) have a nontrivial solution. For an approximate calculation, taking equations up to $n=2$, the smallest eigenvalue is obtained as

$$\lambda_s=\frac{(1-\nu^2)\phi_m^2}{\psi_1^2+(\psi_1^2+\phi_m^2)^2+(3+2\nu)\phi_m^2} \quad (12)$$

Furthermore, assuming

$$mb/a\ll 1 \quad (13)$$

then Eq. (12) is reduced to

$$\lambda_s=\frac{(1-\nu^2)\kappa^4}{1+\kappa^2}\frac{1}{Z^2} \quad (14)$$

with

$$Z=a/m\pi R \quad (15)$$

Antisymmetric Buckling

In this case the governing equations are

$$\frac{\bar{a}_{n-2}}{4}+[1-A_n+\alpha(\phi_m^2+\psi_n^2)^2-\lambda_m]\bar{a}_n+\frac{\bar{a}_{n+2}}{4}-\frac{\nu\phi_m\bar{b}_{n-1}}{2} -\frac{\nu\phi_m\bar{b}_{n+1}}{2}-\frac{\psi_{n-1}\bar{c}_{n-1}}{2}-\frac{\psi_{n+1}\bar{c}_{n+1}}{2}=0 \quad (n=1,2,3,\ldots) \quad (16)$$

$$-\frac{\nu\phi_m\bar{a}_{n-1}}{2}-\frac{\nu\phi_m\bar{a}_{n+1}}{2}+\left[\phi_m^2+\frac{(1-\nu)\psi_n^2}{2}-\lambda_m\right]\bar{b}_n +\frac{(1+\nu)\phi_m\psi_n\bar{c}_n}{2}=0 \quad (n=1,2,3,\ldots) \quad (17)$$

$$-\frac{\psi_n\bar{a}_{n-1}}{2}-\frac{\psi_n\bar{a}_{n+1}}{2}+\frac{(1+\nu)\phi_m\psi_n\bar{b}_n}{2} +\left[\psi_\eta^2+\frac{(1-\nu)\phi_m^2}{2}-\lambda_m\right]\bar{c}_n=0 \quad (n=1,2,3,\ldots) \quad (18)$$

Taking the terms to $n=3$, the buckling condition is obtained by equating the 9×9 determinant of the coefficient matrix of Eqs. (16-18) to zero, which becomes

$$\lambda_a=\frac{(1-\nu^2)\phi_m^2}{(\phi_m^2+\psi_2^2)(1+4\phi_m^2+4\psi_2^2)}+4\alpha\frac{(\phi_m^2+\psi_2^2)(\phi_m^2+\psi_1^2)^2}{\phi_m^2(1+4\phi_m^2+4\psi_2^2)} \quad (19)$$

Assuming that

$$mb/a\ll 1$$

Eq. (19) can be simplified to

$$\lambda_a=\frac{(1-\nu^2)\kappa^4}{4(16+\kappa^2)}\frac{1}{Z^2}+\alpha\frac{16Z^2}{(16+\kappa^2)\kappa^4} \quad (20)$$

Furthermore, the smallest value of Eq. (20) is obtained when

$$Z^2=[(1-\nu^2)/\alpha]^{1/2}\kappa^4/8 \quad (21)$$

and the corresponding lower bound σ^* for the critical stress is expressed as

$$\frac{\sigma^*}{\sigma_{CL}}=\frac{2}{16+(b/\pi R)^2} \quad (22)$$

where σ_{CL} is the classical buckling stress for a complete circular cylinder under axial compression. Therefore, it is seen that the lower bound σ^* for the antisymmetric buckling stress of a corrugated plate is less than one-eighth that of the classical buckling stress σ_{CL}. The values of Eqs. (14) and (20) are easily obtained using a commercial hand calculator. One example is shown in Fig. 2 for corrugated plates with $h/p=0.916$ and $t/p=0.0134$.

Conclusion

The buckling of a sinusoidally corrugated plate under axial compression has been analytically examined. For a long plate, symmetric buckling occurs at the stress given by Eq. (14). If the plate length becomes short, the antisymmetric buckling becomes critical. The lower bound for antisymmetric buckling stress of Eq. (20) is less than one-eighth that of a classical buckling stress for a circular cylindrical shell.

References

[1] Libove, C., "Buckling of Corrugated Plates in Shear," *Stability of Structures under Static and Dynamic Loads,* ASCE, New York, 1977, pp. 453-462.

[2] Perel, D. and Libove, C., "Elastic Buckling of Infinitely Long Trapezoidally Corrugated Plates in Shear," *Transactions of ASME,* Ser. E, Vol. 45, No. 3, 1978, pp. 579-582.

[3] Sanbongi, S., "Elastic Buckling Analysis of Corrugated Plates under Uniform Compression," National Aerospace Laboratory, Tokyo, Rept. TR-604, 1980 (in Japanese).

[4] Sanbongi, S., "Elastic Buckling Analysis of Corrugated Plates in Shear," *Proceedings of the JSASS/JSME 22nd Structures Conference,* Sendai, Japan, 1979, pp. 180-183 (in Japanese).